α-unbound levels in ^{34}Ar from ^{36}Ar$(p,t)^{34}$Ar reaction measurements and implications for the astrophysical ^{30}S$(\alpha,p)^{33}$Cl reaction rate

A. M. Long,[1,*] T. Adachi,[2] M. Beard,[1] G. P. A. Berg,[1] M. Couder,[1] R. J. deBoer,[1] M. Dozono,[3] J. Görres,[1] H. Fujita,[4] Y. Fujita,[5,4] K. Hatanaka,[4] D. Ishikawa,[4] T. Kubo,[6] H. Matsubara,[4] Y. Namiki,[6] S. O'Brien,[1] Y. Ohkuma,[6] H. Okamura,[4] H. J. Ong,[4] D. Patel,[1] Y. Sakemi,[7] Y. Shimbara,[6] S. Suzuki,[6] R. Talwar,[1,†] A. Tamii,[4] A. Volya,[8] T. Wakasa,[3] R. Watanabe,[6] M. Wiescher,[1] R. Yamada,[6] and J. Zenihiro[4]

[1]*Department of Physics and the Joint Institute for Nuclear Astrophysics, University of Notre Dame, Notre Dame, Indiana 46556, USA*
[2]*Research Center for Electron Photon Science, Tohoku University, Taihaku-ku, Sendai, Miyagi 982-0826, Japan*
[3]*Department of Physics, Kyushu University, Fukuoka 812-8581, Japan*
[4]*Research Center for Nuclear Physics, Osaka University, Ibaraki, Osaka 567-0047, Japan*
[5]*Department of Physics, Osaka University, Toyonaka, Osaka 567-0047, Japan*
[6]*Graduate School of Science and Technology, Niigata University, Niigata, Niigata 950-2181, Japan*
[7]*CYRIC, Tohoku University, Miyagi, Sendai 980-8578, Japan*
[8]*Department of Physics, Florida State University, Tallahassee, Florida 32306, USA*

(Received 15 December 2017; published 22 May 2018)

The ^{30}S$(\alpha,p)^{33}$Cl reaction has been identified in several type-1 x-ray burst (XRB) sensitivity studies as a significant reaction within the αp process, possibly influencing not only the abundances of burst ashes but also the bolometric shape of double-peaked light curves coming from certain XRB systems. Given the dearth of experimental data on the ^{30}S(α,p) ^{33}Cl reaction at burst temperatures, we have performed high energy-resolution forward-angle ^{36}Ar$(p,t)^{34}$Ar measurements in order to identify levels in ^{34}Ar that could appear as resonances in the ^{30}S$(\alpha,p)^{33}$Cl reaction. Energies of levels identified in this work, along with model-based assumptions for spin assignments and spectroscopic factors, were then used to determine a rate for the ^{30}S$(\alpha,p)^{33}$Cl reaction based on a narrow-resonance formalism. The rates determined in this work are then compared with two standard Hauser-Feshbach model predictions over a range of XRB temperatures.

DOI: 10.1103/PhysRevC.97.054613

I. INTRODUCTION

Shortly after their discovery in 1976 [1], type 1 x-ray bursts (XRBs) were determined to be thermonuclear runaways occurring on the surface of neutron stars in binary systems with H/He-rich companion stars [2–4]. As material accumulates, temperatures and densities begin to increase within the accreted envelope. Ultimately, a critical point is reached triggering a thermonuclear runaway fueled by the freshly accreted H and He. During this process the nuclear flow through the *sd* shell is driven by two processes, the *rp* process and the αp process [5]. Depending on peak-burst temperatures, highly temperature-dependent α-capture reactions within the αp process may act as a bypass for some of the lower mass waiting points in the *rp* process. Starting with the breakout from the hot-CNO cycles, the main αp-reaction flow can be written as ^{18}Ne(α,p) ^{21}Na(p,γ) ^{22}Mg(α,p) ^{25}Al(p,γ) ^{26}Si(α,p) ^{29}P(p,γ) ^{30}S(α,p) ^{33}Cl(p,γ) ^{34}Ar(α,p) ^{37}K(p,γ) ^{38}Ca(α,p) ^{41}Sc$(p,\gamma)^{42}$Ti.

Previously, several sensitivity studies (most notably Refs. [6–8]) have shown that the strength of the ^{30}S$(\alpha,p)^{33}$Cl reaction can influence not only the energy output of XRBs but also the final abundances of the burst's ashes. One of the more salient results by Fisker *et al.* [7], was the observed correlation between the strength of the ^{30}S$(\alpha,p)^{33}$Cl reaction rate and the double-peaked structure observed in their simulated light curves. The results of this study suggested that given a relatively weak (α,p) rate the nuclear flow would stall at ^{30}S, thus resulting in an observable delay in the rise time that could account for the double-peak structure detected in some XRB light curves [9–11].

The ^{30}S$(\alpha,p)^{33}$Cl reaction has proven difficult to experimentally measure, both directly or indirectly. Because of this, there exists very little experimental information on the reaction, especially at XRB temperatures. Currently, the only previously published work was Deibel *et al.* [12], who studied the time reversal reaction ^{33}Cl$(p,\alpha)^{30}$S and was able to report a converted cross section at three points over an energy range of $E_{c.m.} \sim 4$–5.3 MeV.

Given the sparsity of experimental information, most XRB sensitivity studies still rely on statistical models, such as the Hauser-Feshbach (HF) model [13], to predict a ^{30}S$(\alpha,p)^{33}$Cl reaction rate. An HF model assumes that there are a sufficient number of levels in the compound nucleus such that cross sections are no longer sensitive to the detailed properties of the respective levels. This assumption allows for the use of energy-averaged quantities, such as transmission coefficients

*Present address: Physics Division, Los Alamos National Laboratory, Los Alamos, New Mexico 87545, USA.
†Present address: Physics Division, Argonne National Laboratory, Argonne, Illinois 60439, USA.

and level densities, to predict the cross section for a given reaction. In order for an HF model prediction to be reliable for a specific astrophysical reaction, there must be a sufficiently high level density at the relevant astrophysical energies within the compound nucleus such that this statistical approach is appropriate. Past studies by Rauscher *et al.* [14] have indicated that at least ten non-overlapping narrow resonances must lie within the effective astrophysical energy window for a particular HF rate to be considered reliable (within 20% accuracy). Given that ^{34}Ar has a relatively low α threshold of 6743.95(22) keV [15], and that only natural parity states will participate as resonances the reaction, this suggests that the statistical approach utilized by HF models may not be suitable for the ^{30}S$(\alpha,p)^{33}$Cl reaction rate at XRB temperatures. More likely, this reaction is governed by the individual properties of a handful of α-unbound states in ^{34}Ar. As such, the strength of the ^{30}S$(\alpha,p)^{33}$Cl reaction depends critically on the specific number and strength of resonances in the compound nucleus of ^{34}Ar.

The excitation energy range in ^{34}Ar that is relevant to observed temperatures in XRBs can be roughly determined using the Gamow window approximation [16]. Starting from breakout temperatures of $T \simeq 0.7$ GK and extending up to peak burst temperatures $T \simeq 2.0$ GK, the corresponding relevant energy range for the ^{30}S$(\alpha,p)^{33}$Cl reaction is calculated to be $E_{c.m.} \sim 1.1$–3.8 MeV (this translates to an excitation energy range in ^{34}Ar of $E_x \sim 7.8$–10.5 MeV).

Previous measurements have identified five α-unbound states in ^{34}Ar [17–19], of which only one falls within the relevant energy range. With this in mind, this work aims to identify possible resonances within the ^{30}S$(\alpha,p)^{33}$Cl reaction by precisely measuring α-unbound states in the compound nucleus (^{34}Ar) by performing ^{36}Ar$(p,t)^{34}$Ar reaction measurements at the Ring Cyclotron Facility of the Research Center for Nuclear Physics (RCNP) at Osaka University.

In this paper we present the level structure of α-unbound states within ^{34}Ar as populated though the ^{36}Ar$(p,t)^{34}$Ar reaction with the main goal of identifying possible resonances in the ^{30}S$(\alpha,p)^{33}$Cl reaction relevant to XRB temperatures. Techniques used and the experimental setup are reviewed in Sec. II. The experimental results are presented in Sec. III. In Sec. IV, the new level information is used to derive a ^{30}S$(\alpha,p)^{33}$Cl reaction rate and compare it to standard HF predicted rates used in XRB models.

II. EXPERIMENTAL TECHNIQUES

The goal of this work was to investigate possible resonances within the ^{30}S$(\alpha,p)^{33}$Cl reaction by identifying α-unbound states in the compound nucleus, ^{34}Ar. Given the possibility of closely spaced resonances, this measurement utilized high energy-resolution forward-angle (p,t) techniques using magnetic spectrographs. These types of high-precision (p,t) reaction techniques have been well developed at both RCNP and iThemba for several indirect (α,p) measurements (see [20–24] and references therein).

A. Experimental setup

For this work at RCNP, a 100-MeV proton beam was produced and delivered via the fully dispersion-matched WS beam line [25] to a target chamber positioned in front of the Grand Raiden spectrograph [26]. At the target chamber, the proton beam impinged upon a gas cell of dimensions 44 mm $\times$ 14 mm $\times$ 10 mm filled with highly enriched ($\geqslant$99%) ^{36}Ar gas. Pressurized to 0.5 atm, this roughly corresponds to a target thickness of 0.76 mg/cm^2. Aramid foils ($C_{14}O_2N_2Cl_2H_8$), each with a thickness of 6 μm, were used as the entrance and exit windows of the gas cell [27]. After exiting the Ar gas cell target, the proton beam, along with the reaction products, were differentiated according to their momenta by the Grand Raiden spectrograph. The beam was collected in a Faraday cup placed inside the first dipole (D1) magnet of Grand Raiden, while the reaction products were further transported to the focal plane detector system. This detector system consisted of two multiwire drift chambers (MWDCs), along with two plastic scintillating detectors. In this setup, horizontal and vertical position and angle information were recorded from the MWDCs (used to reconstruct reaction kinematics), while ΔE and time-of-flight information was collected from the plastic scintillators (used for particle identification and background reduction).

Dispersion matching techniques, as described in Refs. [28] and [29], were used to achieve high energy resolution ($\sim$30 keV) in the focal plane. Background contaminants coming from reactions on the gas cell's aramid foils (mostly from ^{12}C and ^{16}O) were identified using an empty gas cell. For this work a full range of excitation energies in ^{34}Ar from the ground state (g.s.) to 11 MeV were investigated. Given a momentum acceptance of the Grand Raiden spectrograph of 5%, an overlapping technique of two different field settings was used to cover the entire energy range up to 11 MeV. Focal plane spectra of both the empty gas cell and the cell filled with ^{36}Ar are shown in Fig. 1. In addition to taking focal plane spectra at multiple field settings, measurements were performed at three scattering angles ($\theta_{\rm lab} = 0^\circ$, 8°, and 11°). By analyzing the kinematic shifts of peaks over the three angles, contaminant peaks could be further separated out from the peak of interest. Largely, in order for a state from ^{34}Ar to be reported in this work, it must be observed in at least two of the three angles recorded.

B. Focal plane calibration and peak fitting

Given the nature of the high-precision energy measurement, great care was taken to calibrate the relationship between the energy of the outgoing tritons and their position on the focal plane. The calibration method used for the focal plane of the Grand Raiden spectrograph follows previous procedures, as described in Refs. [20,21,24]. An absolute energy calibration of the focal plane was obtained using well-known low-lying states in ^{22}Mg populated by the ^{24}Mg(p,t) reaction (g.s. up to 6.226 MeV in excitation energy). In addition, well known energy values of 0^+ and 2^+ states in ^{34}Ar were used to extrapolate this energy calibration to focal plane spectra taken at all angles and magnetic field settings (see Table I).

All peaks that were identified in focal spectra were fit with symmetric Gaussian distributions, where the position of each peak was taken as the centroid of the fit. Isolated peaks were fit with a single Gaussian plus a linear background function,

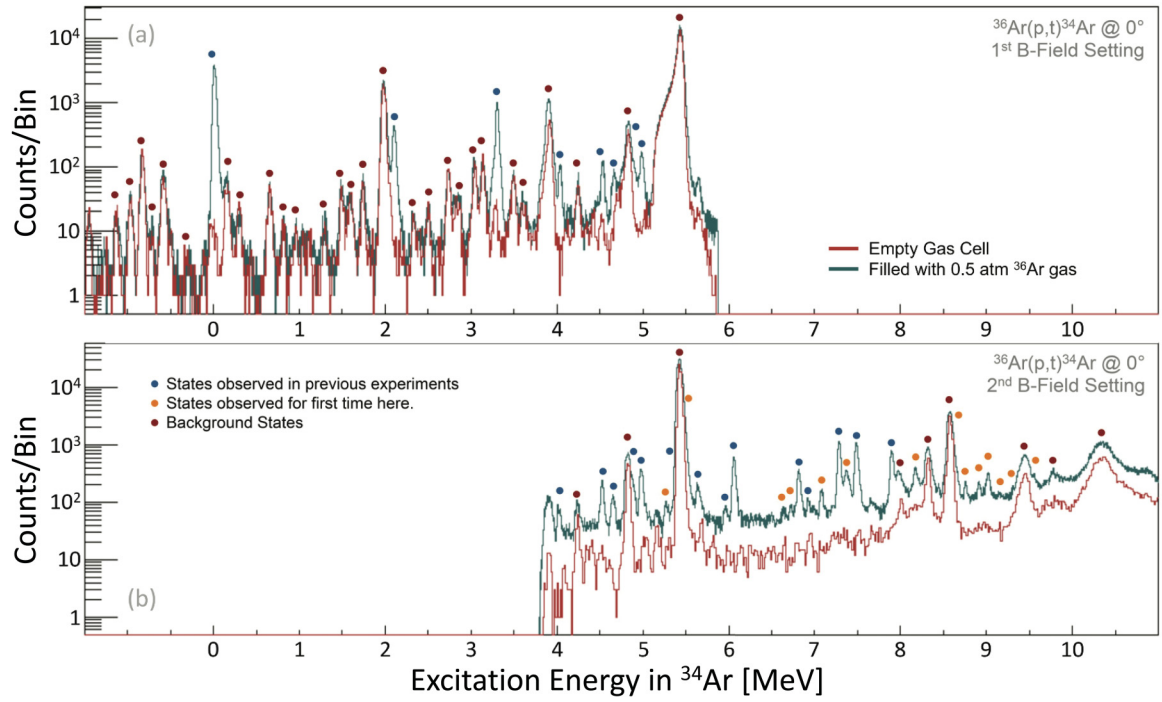

FIG. 1. ^{34}Ar spectra as seen in the focal plane of the Grand Raiden spectrograph at $\theta_{lab} = 0^\circ$ for two different magnetic field settings [panels (a) and (b)]. With these two magnetic field settings a full energy region from the g.s. to 11 MeV in excitation energy is covered in ^{34}Ar. Both spectra shown have been gated on energy loss and time of flight. Additionally, an empty gas cell spectrum has been included (normalized to the ^{10}C g.s peak located at ∼5.3 MeV) to show possible sources of contamination peaks. Each peak has been labeled according to whether it has been identified as background (red online), has been observed in previous works (blue online), or has been observed for the first time in this work (orange online). Additional spectra were recorded at $\theta_{lab} = 8^\circ$ and 11° to help separate background peaks from peaks of interest in ^{34}Ar.

TABLE I. States identified below the α threshold, along with previous (p,t) and $(^3\text{He},n)$ experiments populating states in ^{34}Ar. Proton and α thresholds are located at 4663.92(40) and 6743.95(22) keV in excitation energy, respectively. All excitation energies are given in keV.

This work	Ref. [17]		Ref. [18]		Ref. [19]		Ref. [30]	
^{36}Ar$(p,t)^{34}$Ar	^{36}Ar$(p,t)^{34}$Ar	J^π	^{36}Ar$(p,t)^{34}$Ar	J^π	^{32}S$(^3\text{He},n)^{34}$Ar	L	^{32}S$(^3\text{He},n)^{34}$Ar	J^π
g.s.[a]	g.s.	0^+	g.s.	0^+	g.s.	0	g.s.	0^+
2091.5(24)[a]	2094(11)	2^+	2097(20)	2^+	2090(30)	2	2091.1(3)	2^+
3290.9(18)[a]	3288(14)	2^+	3303(25)	2^+	3290(30)	(2)	3287.7(5)	(2^+)
3878.8(33)[a]	3879(15)	0^+	3899(25)	0^+	3900(70)	(0)	3873(3)	0^+
4019.1(43)	4050(15)							
							4127.8(10)	
4514.9(23)	4522(14)		4560(40)	(3^-)	4510(30)	3	4513.2(8)	3^-
4641.3(21)	4651(14)							
4875.9(38)	4867(14)							
4967.2(27)	4985(14)		4970(40)	0^+	4950(50)	0		
5262(15)								
5330(17)	5307(13)		5340(40)		5310(30)	5		
5535(18)[b]								
5629.6(45)					5620(30)	2		
5948.2(66)	5909(12)				5930(50)	0		
6049.2(20)	6074(11)		6100(40)	2^+				
	6525(9)				6470(30)			
6641(14)								
6723(22)								

[a]States in ^{34}Ar used to match spectra at each angle to absolute calibration.
[b]State observed at only $\theta_{lab} = 11^\circ$.

while groups of closely spaced peaks were fit with multiple Gaussians plus a linear background simultaneously.

All final uncertainties in the energy of levels identified in this work are given by a combination of systematic and statistical uncertainties, added quadratically. Sources of systematic uncertainties include the focal plane energy calibration, the reaction angle determination ($\pm 0.1^\circ$), the ^{36}Ar$(p,t)^{34}$Ar reaction Q value ($\pm$0.08 keV based on [15]), and the effective target thickness of the gas cell ($\pm$0.08 mg/cm^2). The statistical uncertainty is given as the full width at half maximum (FWHM) divided by the area calculated by the Gaussian fit for each peak.

III. EXPERIMENTAL RESULTS

In this work, a total of 32 states were identified in ^{34}Ar, of which seven states were observed below the proton threshold of 4663.92(40) keV [15], ten states were observed between the proton and α threshold, 6743.95(22) keV [15], and 15 states were observed above the α threshold up to $\sim$9.5 MeV in excitation energy. Of these 32 states, a total of 14 states were observed for the first time in this work.

A. States below the α threshold

Prior to this work, four other experiments probed states in ^{34}Ar [17–19,30]. States below the α threshold populated through the ^{36}Ar$(p,t)^{34}$Ar reaction in this work are listed in Table I, along with the states observed in previous works. In this work, the well-known g.s., 2091.5-, 3290.9-, and 3878.8-keV states were used to match the absolute energy calibration of the focal plane to ^{34}Ar spectra taken at each of the three scattering angles ($\theta_{\rm lab} = 0^\circ$, 8°, and 11°). Of the states observed below the α threshold, most agree well with previous works with the exception of the states located at 4019.1(43), 5948.2(66), and 6049.2(20) keV in excitation energy. Both the 4019.1(43)- and 6049.2(20)-keV states are slightly lower than what has been previously reported, 4050(15) [17] and 6074(11) [17] or 6100(40) keV [18], respectively. The 5948.2(66)-keV state is slightly higher than the values of 5909(12) and 5930(50) keV previously reported by Paddock *et al.* [17] and Alford *et al.* [19], respectively. Additionally, there are four states at 5262(15), 5535(18), 6641(14), and 6723(22) keV, that have been observed for the first time in this work. It should be noted that the 5535(18)-keV state was observed only at one angle, $\theta_{\rm lab} = 11^\circ$, as this energy region was obscured by background peaks in the $\theta_{\rm lab} = 0^\circ$ and 8° spectra.

B. States above the α threshold

Prior to this work only five states had been reported above the α threshold. In this work, four of the previously reported states have been confirmed. The 6990(50)-keV state reported by [19] was not observed in this work, though, a state was observed at 6917(5) keV, which lies near the lower limit of its reported error. Given their close proximity when accounting for uncertainties, it was decided to treat these as the same state. In addition to the previously reported states, ten states have been observed for the first time. All states observed in this work, along with states reported from previous works, are listed in Table II. States listed in Table II, with the exception of two, were observed in at least two of the three scattering angles. The two exceptions are the 8660(9)- and 8899(8)-keV states, which were only observed at a single angle ($\theta_{\rm lab} = 11^\circ$ and $\theta_{\rm lab} = 0^\circ$, respectively). This was due to background peaks from the aramid windows dominating the spectra within these energy regions. These two states (displayed with an asterisk in Table II) were included in the final results as they exhibited the same kinematic shift in energy, within the horizontal angle acceptance of the Grand Raiden spectrograph, as all other ^{34}Ar states.

TABLE II. Observed α-unbound states in this work, along with previous (p,t) [17,18] and (^{3}He,n) [19] experiments identifying α-unbound states in ^{34}Ar. All excitation energies are given in keV. Peaks followed by asterisks (*) were identified in only one of the three angles.

This work ^{40}Ca(p,t)	Ref. [17] ^{40}Ca(p,t)	Ref. [18] ^{40}Ca(p,t)	Ref. [19] ^{36}Ar(^{3}He,n)
6808(3)	6794(11)	6860(40)	6820(40)
6917(5)			6990(50)
7072(8)			
7276(2)			
7358(4)	7322(6)	7340(50)	7300(30)
7476(2)	7499(4)	7530(50)	
7889(2)	7925(5)	7950(50)	
8166(3)			
8660(9)*			
8746(8)			
8899(8)*			
9004(4)			
9148(22)			
9226(18)			
9549(16)			

IV. ^{30}S$(\alpha,p)^{33}$Cl REACTION RATE

As stated in Sec. I, the ^{30}S$(\alpha,p)^{33}$Cl reaction is thought to play an important role the nuclear flow through the *sd* shell during type-1 XRBs. Given the relatively long β-decay half-life of ^{30}S, 1.178(5) s [31], along with a relatively low (p,γ) Q value of 264.27(345) keV [15], suggests that ^{30}S is a waiting point for nuclear flow through the *sd* shell in the *rp* process. Depending on its strength, the ^{30}S$(\alpha,p)^{33}$Cl reaction within the αp process may act as a bypass for nuclear material building up at ^{30}S. Given this notion, the possibility of the nuclear flow stalling at ^{30}S depends uniquely on the reaction strength of ^{30}S$(\alpha,p)^{33}$Cl.

Given the small amount of experimental data on the ^{30}S$(\alpha,p)^{33}$Cl reaction, the rate is still based on HF model predictions. With this in mind, this work aims to indirectly measure this rate by probing states in ^{34}Ar that will act as resonances. Given that the only states that will participate in the ^{30}S$(\alpha,p)^{33}$Cl reaction are of natural parity, the ^{36}Ar(p,t) reaction at $E_p = 100$ MeV was chosen to populate states in ^{34}Ar. The (p,t) reaction at high incoming energies is considered to be dominated by a one-step two-particle spin-zero transfer process at very forward angles [17,32], thus this

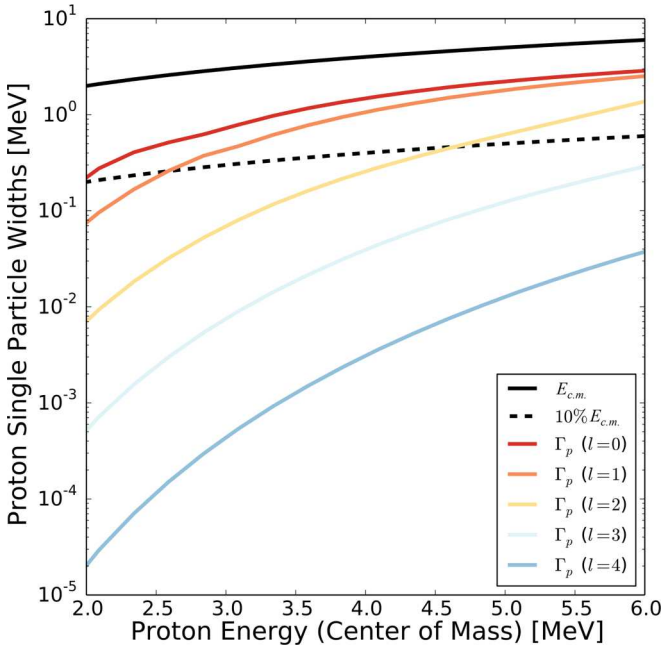

FIG. 2. Calculated proton particle widths in the ^{33}Cl + p system as a function of center-of-mass energy, for a given range of orbital angular momenta, ℓ = 0–4. A proton center-of-mass energy range of 3.2–6 MeV approximately corresponds to an excitation energy range of 7.8–10.6 MeV in ^{34}Ar.

reaction mechanism would selectivity populate natural parity states in ^{34}Ar. We therefore assume all states observed in this work to be of natural parity.

A. Narrow-resonance reaction rate formalism

Within the energy range of interest, total resonance widths, taken as the sum of all open channel partial widths ($\Gamma_{\rm tot} = \Gamma_\alpha + \Gamma_p + \Gamma_\gamma$), will be dominated by the proton partial width. At a given incoming energy, α partial widths will be considerably smaller than corresponding proton partial widths due to an ever increasing Coulomb barrier for low energy α particles. Additionally, γ widths (Γ_γ) in this energy region are at most on the order of eV, and therefore much smaller than the corresponding proton width. Taking these considerations into account, the total resonance width can be approximated as just the proton partial width ($\Gamma_{\rm tot} \simeq \Gamma_p$).

The resonance conditions within the relevant excitation energy (E_x = 7.8–10.5 MeV) in ^{34}Ar are illustrated in Fig. 2. Here, proton single-particle widths, Γ_p^{sp}, are plotted as a function of proton center-of-mass energy given a range of orbital angular momenta, l = 0–4. Modern shell model calculations, using interaction Hamiltonians laid out in [33–35], have shown that proton spectroscopic factors for states in this relevant energy region are on the order of C^2S_p = 0.1–0.01. Calculating proton partial widths for a given states as $\Gamma_p = C^2S_p\ \Gamma_p^{sp}$, it is clear that most of these states, if resonances, can be considered narrow ($\Gamma_{\rm tot} \simeq \Gamma_p \leqslant 10\%\ E_{\rm res}$ [36]).

The above conditions allow us to adopt a narrow-resonance formalism to calculate the total ^{30}S$(\alpha,p)^{33}$Cl reaction rate over a range of XRB temperatures. For a thorough review of this formalism, see Ref. [16]. Within this formalism, the total reaction rate is expressed as a sum of the reaction rate contributions from individual resonances i:

$$N_A\langle\sigma\nu\rangle = 1.54\times10^{11}(\mu T_9)^{-3/2} \times\sum_i(\omega\gamma)_i\exp\left(\frac{-11.605E_i}{T_9}\right), \quad (1)$$

where μ is the reduced mass (amu), T_9 is the temperature (10^9 K), $(\omega\gamma)$ is the resonance strength (MeV), and E_i is the resonance energy in the center-of-mass system (MeV). The resonance strength is defined as

$$(\omega\gamma)_i = \frac{2J_i+1}{(2j_1+1)(2j_2+1)}\frac{\Gamma_a\Gamma_b}{\Gamma_{\rm tot}}. \quad (2)$$

Here, J_i, j_1, and j_2 are the spins of the level, projectile, and target, respectively. Γ_a and Γ_b are the partial widths for the formation and decay of the compound nucleus, respectively, and $\Gamma_{\rm tot}$ is the total width of the state. In the case of the ^{30}S$(\alpha,p)^{33}$Cl reaction, J_i, $j_1 = j_\alpha = 0$, and $j_2 = j_{(^{30}S)} = 0$ are the total angular momenta of the level, the α particle, and ^{30}S, respectively. For the partial widths, $\Gamma_a = \Gamma_\alpha$ and $\Gamma_b = \Gamma_p$, with the total width being $\Gamma_{\rm tot} = \Gamma_\alpha + \Gamma_p + \Gamma_\gamma$. As discussed, the total widths of these resonances will be dominated by the proton-partial widths ($\Gamma_p \gg \Gamma_\alpha$ and Γ_γ, therefore $\Gamma_{\rm tot} \simeq \Gamma_p$). With this approximation, Eq. (2) simplifies to

$$(\omega\gamma)_i \approx (2J_i+1)\Gamma_\alpha. \quad (3)$$

The α partial width can be given as

$$\Gamma_\alpha = C^2S_\alpha\Gamma_\alpha^{sp}. \quad (4)$$

Here, C^2 is the Clebsch-Gordan coefficient, S_α is the α-spectroscopic factor, and Γ_α^{sp} is the α single-particle width.

Unfortunately, there is very little experimental information on spins and α-spectroscopic factors (α SFs) for states above the α threshold, with the exception of two states, 7358(4) and 7476(2) keV, where [18] identified their spin parities to be most likely 2^+. Given that most spins and α-spectroscopic factors above the α threshold are experimentally unknown, various models are utilized in order to fill in this missing information needed to calculate a total reaction rate.

B. Treatment of unknown spin assignments and α-spectroscopic factors

In order to obtain the missing information on spins of states above the α threshold in ^{34}Ar, a random sampling procedure from spin distributions derived using a back-shifted Fermi gas (BSFG) model [37] was utilized. For further review on how the BSFG model was implemented to obtain spin values for each state, see [24] and references therein. Given the relevant excitation energy range, calculated spin distributions (illustrated in Fig. 3) highly favor lower spins, peaking roughly around J = 1 for most excitation energies.

Additionally, no experimental information exists on α SFs for states above the α threshold in ^{34}Ar. Given that α partial widths, and therefore α SFs, impact the reaction rate through the resonance strengths of each state, the assumptions made in determining these missing α SFs become critical in calculating

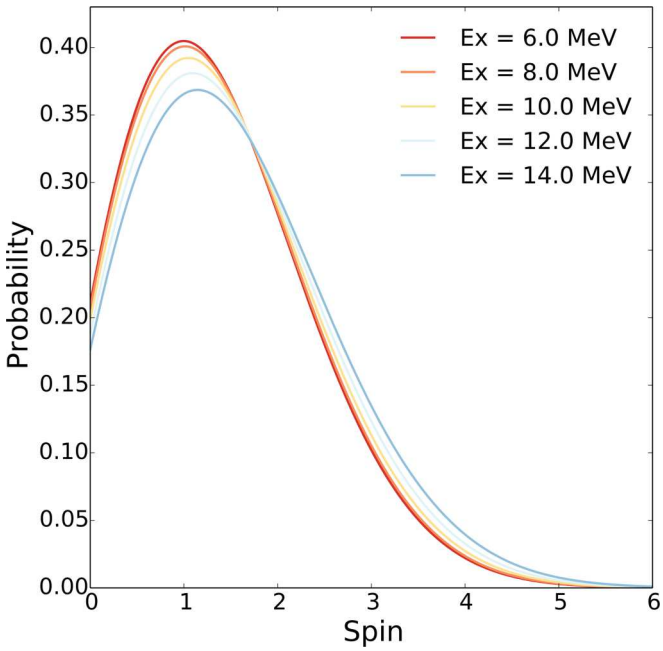

FIG. 3. Spin distributions for selected excitation energies in ^{34}Ar based on the BSFG parameters used in TALYS 1.8. [38].

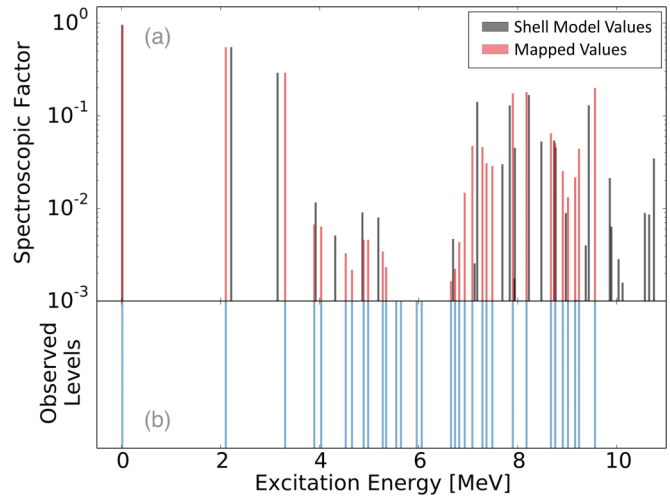

FIG. 4. (a) α-spectroscopic factors for states in ^{34}Ar calculated using the shell model as described in [44] (shown in gray), along with the mapped values to states observed in this work (overlaid). (b) Level density of observed states in ^{34}Ar from this work and previous works.

the resultant ^{30}S$(\alpha,p)^{33}$Cl reaction rate. In keeping with the previous work of [24], two sets of α-SF values were utilized in order to explore the possible effects of α-cluster states above the α threshold in ^{34}Ar.

Previous experimental studies using α-transfer and knock-out reactions have examined α-particle SFs for low-lying states in a handful of nuclei within the *sd* shell [39–43], showing significant α-cluster structure in the states observed. In order to represent the possibility of α-cluster states in ^{34}Ar above the α threshold, α-SF values were calculated using a cluster-nucleon configuration interaction model [44]. In this calculation, the traditional shell model approach was extended using shell model Hamiltonians from [34] and states with up to two particle-hole excitations. For further review see [44] and references therein. Calculated α SFs using this extended shell model by Volya *et al.* [44] are illustrated in Fig. 4. Examining Fig. 4, it is clear that this type of shell model calculation predicts a hierarchy of states based on their α-SF values. In this case, the total ^{30}S$(\alpha,p)^{33}$Cl reaction rate would be dominated by a handful of strong α-cluster-like states above the α threshold.

Given that most of the shell-model calculated excitation energies do not exactly line up with the experimentally observed states in this work, shell model α-SF values are mapped onto the observed states using Gaussian smoothing functions. For a review of this mapping procedure, see [24]. The results of this mapping (using a smearing width of $\sigma = 150$ keV) are illustrated in Fig. 4 (shown in red).

In the case of non-α-cluster-like states, a global value of $S_\alpha = 0.01$ was taken for all α-unbound states, thus representing the case where all α partial widths would be $\sim$1% of the total single α-particle width (Γ_α^{sp}).

This global value was used as it has been historically assigned as a typical value for states where α SFs are not known [45,46]. Additionally, it also follows the values chosen in previous works performing similar (α,p) reaction rate calculations [21,22,24]. Calculating a total reaction rate given this global value of $S_\alpha = 0.01$ serves mainly two purposes: first, this value may fall closer to what would be seen in statistical models where averaged values represent strengths fractured over many, many states. The use of this global value allows for a first-order comparison with statistical models, thus exploring the question of whether there are enough levels in ^{34}Ar to justify a statistical approach. Second, we can then compare to the total rate derived using the α-SF values representing the possibility of α clustering. This comparison allows us to investigate the effects α-cluster-like states would have on the ^{30}S$(\alpha,p)^{33}$Cl rate in a stellar environment like XRBs.

C. Calculating the total rate

Given the information of possible resonance energies from levels observed in this work, along with the assumptions made to calculated spins and α SFs, a Monte Carlo calculation was performed based on Eq. (1). To begin, each state is randomly given a spin based on the distributions generated by the BSFG model using the rejection-acceptance method [47].

Once a particular set of spins was assigned, α single-particle widths were calculated for each state using the BIND subroutine in the DWUCK4 code [48]. For further information on this code and how it generates single-particle widths see the Appendix of [24,49]. With α single-particle widths calculated, α partial widths were then determined using Eq. (4) with a given set of α-SF values. Given this set of spins and α partial widths, resonance strengths were determined using Eq. (3) for all states. Finally the total ^{30}S$(\alpha,p)^{33}$Cl reaction rate was calculated using Eq. (1).

This total rate calculation was performed $N = 10^7$ times with different spin-set combinations, thus producing a

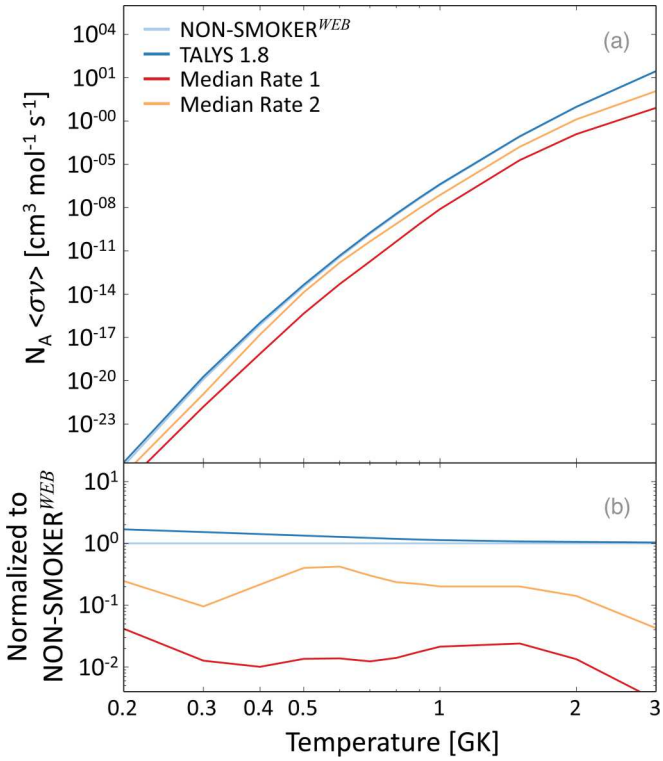

FIG. 5. (a) The two median ^{30}S$(\alpha,p)^{33}$Cl reaction rates as a function of stellar temperature calculated in this work, median rate 1 (non-α clustering) and median rate 2 (with α clustering), along with statistical model calculated rates, NON-SMOKER$^{\text{WEB}}$ v5.0w and TALYS 1.8. (b) All rates are normalized to the NON-SMOKER$^{\text{WEB}}$ v5.0w rate.

distribution of total rates at a given temperature. Total rate distributions were calculated over a range of temperatures relevant to XRBs, where at each selected temperature value, a median rate was determined by calculating the 0.50 quantile of the rate distribution. Finally, it is this median rate value that is quoted as the total ^{30}S$(\alpha,p)^{33}$Cl reaction rate for this work. This Monte Carlo rate calculation is plotted as a function of temperature in Fig. 5. For XRB light curves, relevant temperatures start at $T \sim 0.7$ GK and extend up to possible peak burst temperatures of $T \sim 2.0$ GK.

As mentioned previously in Sec. IV B, this total rate calculation was performed given two different sets of α-SF values, once with the mapped shell model α SFs, representing the possibility of α-cluster states in ^{34}Ar, and again with global α-SF values of $S_\alpha = 0.01$, representing the possibility of no α-cluster states in ^{34}Ar above the α threshold. In Fig. 5, the latter is labeled as "Median Rate 1," while the former is labeled as "Median Rate 2."

For comparison with HF predictions, two HF model predicted rates from NON-SMOKER$^{\text{WEB}}$ v5.0w [50] and TALYS 1.8 [38] are also plotted in Fig. 5. Both median rates from this work, along with the two HF model predictions, are listed in Table III, for further comparison at, and slightly beyond, observed XRB temperatures.

As seen in Fig. 5, throughout the temperature range relevant to XRBs, both median rates from this work are lower than the HF predictions of NON-SMOKER$^{\text{WEB}}$ v5.0w and TALYS 1.8. A comparison of median rate 1 to the HF predicted rates suggests that the level density above the α threshold in ^{34}Ar, as observed in this work, is not high enough to support the statistical approach used by HF models. This comparison brings into question the reliability of using a HF model to predict the ^{30}S$(\alpha,p)^{33}$Cl reaction rate at observed XRB temperatures. Furthermore, the overall shape of median rate 2, along with its roughly order of magnitude discrepancy with median rate 1, illustrates the influence that possible α-clustering states would have on the total reaction rate. At some temperatures in Fig. 5, such as ~0.5 GK, median rate 2 is much closer to HF predictions not because there are many states contributing in a statistical manner, but because there are one or two α-cluster-like states dominating the total reaction rate. Finally, the dip in the reaction rate around $T \sim 1.5$ GK comes from a

TABLE III. The total reaction rate $N_A\langle\sigma\nu\rangle$, in units of cm^3 mole^{-1} sec^{-1}, as a function of temperature from the narrow-resonance calculation based on this work. Listed are the resultant median rates from this work, meant to account for the possibilities of α-clustering and non-α-clustering, along with two standard HF model predictions from NON-SMOKER$^{\text{WEB}}$ v5.0w and TALYS 1.8 for comparison.

Temperature (GK)	NON-SMOKER$^{\text{WEB}}$ v5.0w	TALYS 1.8	Median rate 1	Median rate 2
0.10	5.49×10^{-39}	3.85×10^{-31}	6.43×10^{-41}	4.97×10^{-40}
0.15	2.14×10^{-31}	2.19×10^{-26}	8.77×10^{-33}	6.15×10^{-32}
0.20	1.30×10^{-26}	5.18×10^{-23}	5.41×10^{-28}	3.20×10^{-27}
0.30	1.26×10^{-20}	1.92×10^{-20}	1.59×10^{-22}	1.20×10^{-21}
0.40	7.30×10^{-17}	1.03×10^{-16}	7.37×10^{-19}	1.57×10^{-17}
0.50	3.40×10^{-14}	4.54×10^{-14}	4.62×10^{-16}	1.36×10^{-14}
0.60	3.62×10^{-12}	4.62×10^{-12}	5.00×10^{-14}	1.53×10^{-12}
0.70	1.49×10^{-10}	1.82×10^{-10}	1.84×10^{-12}	4.49×10^{-11}
0.80	3.14×10^{-09}	3.72×10^{-09}	4.42×10^{-11}	7.42×10^{-10}
0.90	4.10×10^{-08}	4.73×10^{-08}	7.24×10^{-10}	9.04×10^{-09}
1.00	3.71×10^{-07}	4.20×10^{-07}	7.94×10^{-09}	7.47×10^{-08}
1.50	8.07×10^{-04}	8.69×10^{-04}	1.94×10^{-05}	1.62×10^{-04}
2.00	9.15×10^{-02}	9.67×10^{-02}	1.23×10^{-03}	1.29×10^{-02}
2.50	$2.43 \times 10^{+00}$	$2.55 \times 10^{+00}$	1.52×10^{-02}	1.95×10^{-01}
3.00	$2.78 \times 10^{+01}$	$2.88 \times 10^{+01}$	8.15×10^{-02}	$1.18 \times 10^{+00}$

lack of observed excited states above 9.5 MeV in ^{34}Ar in this work. At peak burst temperatures of 2 GK, the Gamow-window extends up to ∼10.5 MeV in excitation energy, and it is very likely that there are additional states in this region not observed in this work that may contribute as resonances. This suggests that further studies are needed in order to identify more possible states above the α threshold, especially in the excitation energy region of 9–11 MeV. It should be noted here that, after submission, within the review process for this work, three new states were identified in ^{34}Ar above 11 MeV by Kahl *et al.* [51] (11.09, 11.52, and 12.08 MeV). These states, though outside the Gamow window for peak burst temperatures, may affect the downward dip observed in Fig. 5.

Overall, given the number of states observed in this work along with the resultant calculated total rates, it is possible that the ^{30}S$(\alpha,p)^{33}$Cl reaction rate, at most XRB temperatures, is governed by a handful of resonances corresponding to levels located within the relevant excitation energy range in ^{34}Ar. Therefore, it is critical for further studies to not only look for more possible states above the α threshold, but to also investigate α strengths of levels observed in this work.

V. CONCLUSIONS

In this work we have presented experimentally measured states in ^{34}Ar up to 9.5 MeV in excitation energy. Given that the reaction mechanism of the ^{36}Ar(p,t) reaction at higher energies will preferentially populate natural parity states in ^{34}Ar, all states observed in this work are believed to participate as resonances in the ^{30}S$(\alpha,p)^{33}$Cl reaction. With precise energy information on these resonances determined from this work, along with model assumptions to fill in the missing information on spin assignments and α-spectroscopic factors, distributions of the total ^{30}S$(\alpha,p)^{33}$Cl reaction rate across XRB temperatures were calculated using a Monte Carlo (varying only spin assignments) approach within a narrow-resonance reaction rate formalism. A median rate, taken as the 50% quantile from each rate distribution at a given temperature, is then quoted as the total ^{30}S$(\alpha,p)^{33}$Cl rate as a function of temperature. This Monte Carlo calculation was performed twice using two different sets of α-SF values in order to explore the possible effects that α clustering above the α threshold in ^{34}Ar would have on the total rate. Both calculated median rates are then compared to the HF model predicted rates, specifically NON-SMOKER$^{\text{WEB}}$ v5.0w and TALYS 1.8. Comparing the median rate 1 to the HF model predicted rates suggests that there may not be enough levels at the relevant energies participating as resonances to reliably support a statistical approach. Additional comparisons between the two median rates highlights the degree to which α clustering above the α threshold has on the total rate. These comparisons further strengthen the notion that the ^{30}S$(\alpha,p)^{33}$Cl reaction rate (at most observed XRB temperatures) is most likely governed by structure effects, where a handful of resonances located within the relevant energy window dominate the total reaction rate. With 15 states identified above the α threshold (ten for the first time in this work), future indirect studies should either focus on searching for additional states, or determining much-needed spin and α-spectroscopic information on the α-unbound states observed in this work.

As stated in previous works similar to this one, the two ^{30}S$(\alpha,p)^{33}$Cl reaction rates quoted here are decidedly dependent on the assumptions made in determining missing information needed to calculate a final rate. Given these assumptions, it should be noted that these resultant rates, similar to the rates derived in [21,22,24], should only be taken as exploratory. These rates are meant to not only be initial comparisons to HF predicted rates, but also investigate the effects of α clustering in ^{34}Ar on the stellar rate.

ACKNOWLEDGMENTS

The authors of this work would like to especially thank the technical staff at RCNP for the help and support during the course of the experiment E305. This work was supported by the National Science Foundation through Grant No. PHY-1068192 and The Joint Institute for Nuclear Astrophysics Center for the Evolution of the Elements through Grants No. PHY-0822648 and No. PHY-1430152. Additionally, this material is based upon work supported by the US Department of Energy, Office of Science, Office of Nuclear Physics, under Grant No. DE-SC0009883.

[1] J. Grindlay, H. Gursky, H. Schnopper, D. R. Parsignault, J. Heise, A. C. Brinkman, and J. Schrijver, Astrophys. J. **205**, L127 (1976).
[2] S. E. Woosley and R. E. Taam, Nature (London) **263**, 101 (1976).
[3] P. C. Joss, Nature (London) **270**, 310 (1977).
[4] D. Q. Lamb and F. K. Lamb, Astrophys. J. **220**, 291 (1978).
[5] R. K. Wallace and S. E. Woosley, Astrophys. J. Suppl. Ser. **45**, 389 (1981).
[6] A. Parikh, J. José, F. Moreno, and C. Iliadis, Astrophys. J. Suppl. Ser. **178**, 110 (2008).
[7] J. Fisker, F.-K. Thielemann, and M. Wiescher, Astrophys. J. **608**, L61 (2004).
[8] R. H. Cyburt, A. M. Amthor, A. Heger, E. Johnson, L. Keek, Z. Meisel, H. Schatz, and K. Smith, Astrophys. J. **830**, 55 (2016); H. Schatz and W.-J. Ong, *ibid.* **844**, 139 (2017).
[9] M. Sztajno, J. van Paradijs, W. H. G. Lewin, J. Trumper, G. Stollman, W. Pietsch, and M. van der Klis, Astrophys. J. **299**, 487 (1985).
[10] W. Penninx, W. H. G. Lewin, and J. van Paradijs, Astrophys. J. **321**, L67 (1987).
[11] E. Kuulkers, J. Homan, M. van der Klis, W. H. G. Lewin, and M. Méndez, Astron. Astrophys. **382**, 947 (2002).
[12] C. M. Deibel, K. E. Rehm, J. M. Figueira, J. P. Greene, C. L. Jiang, B. P. Kay, H. Y. Lee, J. C. Lighthall, S. T. Marley, R. C. Pardo, N. Patel, M. Paul, C. Ugalde, A. Woodard, A. H. Wuosmaa, and G. Zinkann, Phys. Rev. C **84**, 045802 (2011).
[13] W. Hauser and H. Feshbach, Phys. Rev. **87**, 366 (1952).
[14] T. Rauscher, F.-K. Thielemann, and K. L. Kratz, Phys. Rev. C **56**, 1613 (1997).

[15] M. Wang, G. Audi, F. G. Kondev, W. J. Huang, S. Naimi, and X. Xu, Chin. Phys. C **41**, 030003 (2017).

[16] C. Iliadis, *Nuclear Physics of Stars*, 2nd ed. (Wiley, New York, 2015).

[17] R. Paddock, Phys. Rev. C **5**, 485 (1972).

[18] H. Brunnader, J. C. Hardy, and J. Cerny, Nucl. Phys. A **137**, 487 (1969).

[19] W. Alford, P. Craig, D. Lind, R. Raymond, J. Ullman, C. Zafiratos, and B. Wildenthal, Nucl. Phys. A **457**, 317 (1986).

[20] A. Matic, A. M. vandenBerg, M. N. Harakeh, H. J. Wörtche, G. P. A. Berg, M. Couder, J. L. Fisker, J. Görres, P. LeBlanc, S. O'Brien, M. Wiescher, K. Fujita, K. Hatanaka, Y. Sakemi, Y. Shimizu, Y. Tameshige, A. Tamii, M. Yosoi, T. Adachi, Y. Fujita *et al.*, Phys. Rev. C **80**, 055804 (2009).

[21] A. Matic, A. M. van den Berg, M. N. Harakeh, H. J. Wörtche, M. Beard, G. P. A. Berg, J. Görres, P. LeBlanc, S. O'Brien, M. Wiescher, K. Fujita, K. Hatanaka, Y. Sakemi, Y. Shimizu, Y. Tameshige, A. Tamii, M. Yosoi, T. Adachi, Y. Fujita, Y. Shimbara *et al.*, Phys. Rev. C **84**, 025801 (2011).

[22] S. Almaraz-Calderon, W. P. Tan, A. Aprahamian, M. Beard, G. P. A. Berg, B. Bucher, M. Couder, J. Görres, S. O'Brien, D. Patel, A. Roberts, K. Sault, M. Wiescher, C. R. Brune, T. N. Massey, K. Fujita, K. Hatanaka, D. Ishiwaka, H. Matsubara, H. Okamura *et al.*, Phys. Rev. C **86**, 065805 (2012).

[23] R. Neveling, H. Fujita, F. D. Smit, T. Adachi, G. P. A. Berg, E. Z. Buthelezi, J. Carter, J. L. Conradie, M. Couder, R. W. Fearick, S. V. Förtsch, D. T. Fourie, Y. Fujita, J. Görres, K. Hatanaka, M. Jingo, A. M. Krumbholz, C. O. Kureba, J. P. Mira, S. H. T. Murray *et al.* Nucl. Instrum. Methods Phys. Res., Sect. A **654**, 29 (2011).

[24] A. M. Long, T. Adachi, M. Beard, G. P. A. Berg, Z. Buthelezi, J. Carter, M. Couder, R. J. deBoer, R. W. Fearick, S. V. Förtsch, J. Görres, J. P. Mira, S. H. T. Murray, R. Neveling, P. Papka, F. D. Smit, E. Sideras-Haddad, J. A. Swartz, R. Talwar, I. T. Usman *et al.*, Phys. Rev. C **95**, 055803 (2017).

[25] T. Wakasa, K. Hatanaka, Y. Fujita, G. P. A. Berg, H. Fujimura, H. Fujita, M. Itoh, J. Kamiya, T. Kawabata, K. Nagayama, T. Noro, H. Sakaguchi, Y. Shimbara, H. Takeda, K. Tamura, H. Ueno, M. Uchida, M. Uraki, and M. Yosoi, Nucl. Instrum. Methods Phys. Res., Sect. A **482**, 79 (2002).

[26] M. Fujiwara, H. Akimune, I. Daito, H. Fujimura, Y. Fujita, K. Hatanaka, H. Ikegami, I. Katayama, K. Nagayama, N. Matsuoka, S. Morinobu, T. Noro, M. Yoshimura, H. Sakaguchi, Y. Sakemi, A. Tamii, and M. Yosoi, Nucl. Instrum. Methods Phys. Res., Sect. A **422**, 484 (1999).

[27] H. Matsubara, A. Tamii, Y. Shimizu, K. Suda, Y. Tameshige, and J. Zenihiro, Nucl. Instrum. Methods Phys. Res., Sect. A **678**, 122 (2012).

[28] Y. Fujita, K. Hatanaka, G. P. A. Berg, K. Hosono, N. Matsuoka, S. Morinobu, T. Noro, M. Sato, K. Tamura, and H. Ueno, Nucl. Instrum. Methods Phys. Res., Sect. B **126**, 274 (1997).

[29] H. Fujita, Y. Fujita, G. P. A. Berg, A. Bacher, C. Foster, K. Hara, K. Hatanaka, T. Kawabata, T. Noro, H. Sakaguchi, Y. Shimbara, T. Shinada, E. Stephenson, H. Ueno, and M. Yosoi, Nucl. Instrum. Methods Phys. Res., Sect. A **484**, 17 (2002).

[30] R. Bell, J. Thompson, I. Graham, and L. Carlson, Nucl. Phys. A **222**, 477 (1974).

[31] M. Shamsuzzoha Basunia, Nucl. Data Sheets **111**, 2331 (2010).

[32] T. Tanabe, K. Haga, M. Yasue, K. Sato, K. Ogino, Y. Kadota, M. Tochi, K. Makino, T. Kitahara, and T. Shiba, Nucl. Phys. A **399**, 241 (1983).

[33] W. A. Richter, S. Mkhize, and B. A. Brown, Phys. Rev. C **78**, 064302 (2008).

[34] E. K. Warburton and B. A. Brown, Phys. Rev. C **46**, 923 (1992).

[35] S. M. Brown, W. N. Catford, J. S. Thomas, B. Fernández-Domínguez, N. A. Orr, M. Labiche, M. Rejmund, N. L. Achouri, H. Al Falou, N. I. Ashwood, D. Beaumel, Y. Blumenfeld, B. A. Brown, R. Chapman, M. Chartier, N. Curtis, G. de France, N. de Sereville, F. Delaunay, A. Drouart *et al.*, Phys. Rev. C **85**, 011302(R) (2012).

[36] C. E. Rolfs and W. S. Rodney, *Cauldrons in the Cosmos: Nuclear Astrophysics* (University of Chicago Press, Chicago, 1988), p. 561.

[37] A. Gilbert and A. G. W. Cameron, Can. J. Phys. **43**, 1446 (1965).

[38] A. J. Koning, in *International Conference on Nuclear Data for Science and Technology*, AIP Conf. Proc. No. 769, edited by R. C. Haight, M. B. Chadwick, T. Kawano, and P. Talou (AIP, Melville, NY, 2005), p. 1154.

[39] T. A. Carey, P. G. Roos, N. S. Chant, A. Nadasen, and H. L. Chen, Phys. Rev. C **29**, 1273 (1984).

[40] T. A. Carey, P. G. Roos, N. S. Chant, A. Nadasen, and H. L. Chen, Phys. Rev. C **23**, 576 (1981).

[41] N. Anantaraman, C. L. Bennett, J. P. Draayer, H. W. Fulbright, H. E. Gove, and J. Tōke, Phys. Rev. Lett. **35**, 1131 (1975).

[42] W. Oelert, W. Chung, M. Betigeri, A. Djaloeis, C. Mayer-Boricke, and P. Turek, Phys. Rev. C **20**, 459 (1979).

[43] W. Oelert, W. Chung, A. Djaloeis, C. Mayer-Boricke, and P. Turek, Phys. Rev. C **22**, 408 (1980).

[44] A. Volya and Y. M. Tchuvil'sky, Phys. Rev. C **91**, 044319 (2015).

[45] C. Iliadis, U. Giesen, J. Görres, S. Graff, M. Wiescher, R. Azuma, J. King, M. Buckby, C. Barnes, and T. Wang, Nucl. Phys. A **533**, 153 (1991).

[46] L. Van Wormer, J. Goörres, C. Iliadis, M. Wiescher, and F.-K. Thielemann, Astrophys. J. **432**, 326 (1994).

[47] W. H. Press, S. A. Teukolsky, W. T. Vetterling, and B. P. Flannery, *Numerical Recipes in C* (Cambridge University Press, Cambridge, England, 1992).

[48] P. D. Kunz, *Zero Range Distorted Wave Born Approximation* (Springer, Berlin, 1984).

[49] C. Iliadis, Nucl. Phys. A **618**, 166 (1997).

[50] T. Rauscher and F.-K. Thielemann, At. Data Nucl. Data Tables **75**, 1 (2000).

[51] D. Kahl, H. Yamaguchi, S. Kubono, A. A. Chen, A. Parikh, D. N. Binh, J. Chen, S. Cherubini, N. N. Duy, T. Hashimoto, S. Hayakawa, N. Iwasa, H. S. Jung, S. Kato, Y. K. Kwon, S. Nishimura, S. Ota, K. Setoodehnia, T. Teranishi, H. Tokieda *et al.*, Phys. Rev. C **97**, 015802 (2018).